Tris(pyridinealdoximato)metal Complexes as Ligands for the Synthesis of Asymmetric Heterodinuclear $Cr^{III}M$ Species [M = Zn(II), Cu(II), Ni(II), Fe(II), Mn(II), Cr(II), Co(III)]: A Magneto−Structural Study

Sylvia Ross, Thomas Weyhermüller, Eckhard Bill, Karl Wieghardt, and Phalguni Chaudhuri*

Max-Planck-Institut für Strahlenchemie, Stiftstrasse 34-36, D-45470 Mülheim an der Ruhr, Germany

Received May 24, 2001

Reactions of the LCr^{III} unit with an in situ prepared $M(PyA)_3^{n-}$ ion, where L represents 1,4,7-trimethyl-1,4,7-triazacyclononane and PyA^- is the monoanion of pyridine-2-aldoxime, yield heterodinuclear complexes of general formula $[LCr^{III}(PyA)_3M]^{2+/3+}$ as perchlorate salts, where M = Cr(II) (**1**), Mn(II) (**2**), low-spin Fe(II) (**3**), Ni(II) (**4**), Cu(II) (**5**), Zn(II) (**6**), and low-spin Co(III) (**7**). These compounds contain three oximato anions as bridging ligands. The hexadentate ligand with the identical donor atoms, tris(2-aldoximato-6-pyridyl)phosphine, $P(PyA)_3$, has been employed to prepare a second $Cr^{III}Ni^{II}$ species **8**, whose magnetic properties differ significantly from those of **4**. Complexes **1**−**8** have been characterized on the basis of elemental analysis, mass spectrometry, IR, UV−vis, Mössbauer, and EPR spectroscopies, and variable-temperature (2−295 K) magnetic susceptibility measurements. They are isostructural in the sense that they all contain a terminal Cr(III) ion in a distorted octahedral environment, CrN_3O_3, and a second six-coordinated metal ion M in a mostly trigonal prismatic MN_6 geometry. The crystal structures of the perchlorate salts of **2**−**5**, **7**, and **8** have been determined by X-ray crystallography at 100 K. The structures consist of mixed-metal $Cr^{III}M^{II}$ and $Cr^{III}Co^{III}$ complexes with a geometry in which two pseudooctahedral polyhedra are joined by three oximato (=N−O$^-$) groups, with an intramolecular Cr···M(Co) distance in the range of 3.4−3.7 Å. The cyclic voltammograms of the complexes reveal ligand oxidation and reduction processes, and in addition, metal-centered oxidation processes have been observed. X-band EPR spectroscopy has been used to establish the electronic ground state of the heterodinuclear complexes. Analysis of the susceptibility data indicates the presence of weak exchange interactions, both ferro- and antiferromagnetic, between the paramagnetic centers. A qualitative rationale on the basis of the Goodenough−Kanamori rules is provided for the difference in magnetic behaviors.

Introduction

This work forms part of our program on exchange-coupled heteropolymetallic systems, whose investigations have been proved to be more informative in comparison to those of homopolynuclear complexes. The ubiquitous participation of metal sites involving more than one metal center in metalloproteins has elicited the interest of bioinorganic chemists in such interactions.[1] We have adopted a synthetic strategy of using metal oximates as ligands for paramagnetic centers to increase the nuclearity and to synthesize heterometallic complexes. Thus a series of dioximato-bridged (diatomic N,O-bridging) linear heterotrinuclear complexes of general formula

$[LM_t\{\mu\text{-(dioxime)}_3M_c\}M_tL]^{2+/4+}$, where M_t = Fe(III),[2] Mn(III),[3] Mn(IV),[4] and Cr(III)[5]

and M_c = Zn(II), Cu(II), Ni(II), Fe(II), and Mn(II),

has been described, where L represents the tridentate cyclic amine 1,4,7-trimethyl-1,4,7-triazacyclononane and dioxime(2−) is the dianion of several oximes. We emphasize in this respect that investigations of a series of isostructural polynuclear complexes with varying d^n-electron configurations are more informative in comparison to those comprising singly isolated, exchange-coupled clusters only.

Applying a very similar strategy, we have succeeded in preparing the asymmetric dinuclear motif $M^{III}\mu(O-N)_3M^{II}$ by using [tris(pyridinealdoximato)metalate(II)]$^-$ anions, $[M(PyA)_3]^-$, as ligands for the LM^{III} unit, where M(III) = Cr(III), Mn(III), Fe(III), and Co(III). In this paper we report the synthesis and spectroscopic and structural characterization of the following LCr^{III}-containing compounds: Here M = Cr(II) (**1**), Mn(II) (**2**),

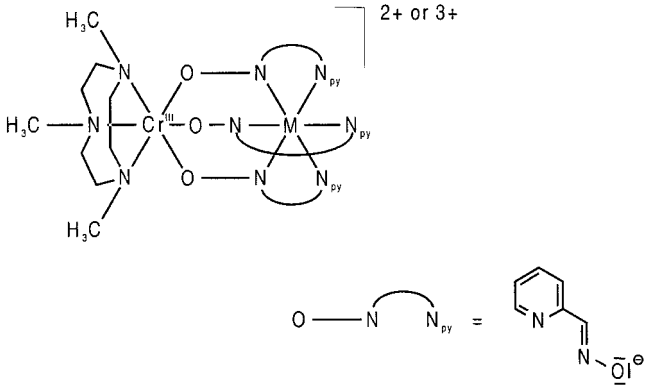

Fe(II) (**3**), Ni(II) (**4**), Cu(II) (**5**), Zn(II) (**6**), and Co(III) (**7**).

* Corresponding author. E-mail: chaudh@mpi-muelheim.mpg.de.

(1) See for example: Holm, R. H., Solomon, E. I., Guest Editors. *Chem. Rev.* **1996**, *96* (7).
(2) Chaudhuri, P.; Winter, M.; Della Vedova, B. P. C.; Fleischhauer, P.; Haase, W.; Flörke, U.; Haupt, H.-J. *Inorg. Chem.* **1991**, *30*, 4777.
(3) Birkelbach, F.; Flörke, U.; Haupt, H.-J.; Butzlaff, C.; Trautwein, A. X.; Wieghardt, K.; Chaudhuri, P. *Inorg. Chem.* **1998**, *37*, 2000.
(4) Birkelbach, F.; Weyhermüller, T.; Lengen, M.; Gerdan, M.; Trautwein, A. X.; Wieghardt, K.; Chaudhuri, P. *J. Chem. Soc., Dalton Trans.* **1997**, 4529.
(5) Burdinski, D.; Bill, E.; Birkelbach, F.; Wieghardt, K.; Chaudhuri, P. *Inorg. Chem.* **2001**, *40*, 1160 and references therein.

10.1021/ic010552y CCC: $20.00
Published on Web 11/10/2001

Throughout this paper the compounds **1**−**7** are denoted by the metal centers only.

To impose trigonal prismatic stereochemistry in six coordinate systems, Holm and co-workers[6] reported the hexadentate ligand tris(2-aldoximato-6-pyridyl)phosphine and its BF encapsulated Ni(II) complex, $[NiP(PyA)_3BF]BF_4$. The twist angle of two N_3 triangles from trigonal prismatic coordination has been reported[7] to be less than ∼2°. Instead of the B-capping unit we used the metal-containing fragment $Cr^{III}L$ for encapsulation of the $[NiP(PyA)_3]$ unit to yield the bicyclic clathrochelate containing the $Cr^{III}Ni^{II}$ to demonstrate how a hexadentate ligand with the identical donor atoms as in the above series can significantly alter the magnetic properties of a heterodimetal complex.

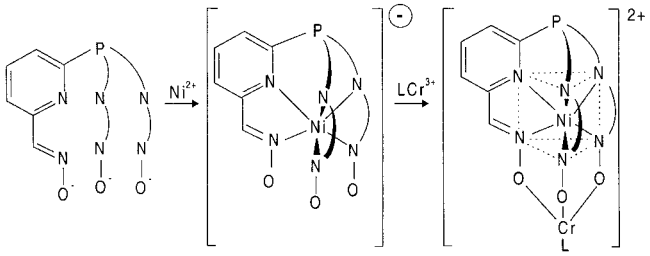

In accord with the predictions made nearly 30 years ago[8] most of the known $Cr^{III}Ni^{II}$ interactions in the literature are ferromagnetic in nature.[9] Examples of such heteronuclear $Cr^{III}Ni^{II}$ are, however, still very limited.[5,10] We report here two $Cr^{III}Ni^{II}$ pairs, **4** and **8**, with identical donor atoms of nearly the same overall structure but exhibiting very different exchange interactions.

Experimental Section

Materials and Physical Measurements. Reagent or analytical grade materials were obtained from commercial suppliers and used without further purification, except those for electrochemical measurements. The macrocycle 1,4,7-trimethyl-1,4,7-triazacyclononane ($C_9H_{21}N_3$ = L) and its chromium(III) complex $LCrBr_3$ were prepared as described previously.[11] Elemental analyses (C, H, N) were performed by the Microanalytical Laboratory Dornis & Kolbe, Mülheim, Germany. Quantitative determination of the metals was performed spectrophotometrically: chromium as chromate at $\lambda = 370$ nm ($\epsilon = 4960$ M^{-1} cm^{-1}) and manganese, iron, and cobalt as their dipicolinic acid complexes.[12] Copper and nickel were determined gravimetrically by using *N*-benzoyl-*N*-phenylhydroxylamine and dimethylglyoxime, respectively. Zinc was determined by AAS. The perchlorate anion was determined gravimetrically as tetraphenylarsonium perchlorate. Fourier transform infrared spectroscopy on KBr pellets was performed on a Perkin-Elmer 2000 FT-IR instrument. Electronic absorption spectra in solution were measured on a Perkin-Elmer Lambda 19 spectrophotometer. Magnetic susceptibilities of *powdered samples* were recorded on a SQUID magnetometer in the temperature range 2−295 K with an applied field of 1 T. Experimental susceptibility data were corrected for the underlying diamagnetism using Pascal's constants. The X-band EPR spectra of the *polycrystalline solid material* or of solution were recorded at various temperatures between 3 and 100 K with a Bruker ESP 300 spectrometer equipped with a standard TE 102 cavity, an Oxford Instruments liquid-helium continuous-flow cryostat, a NMR gaussmeter, a frequency meter, and a data acquisition system. The Mössbauer spectrometer worked in the conventional constant-acceleration mode with a $^{57}Co/Rh$ source. Isomer shifts are given relative to α-Fe at room temperature. Cyclic voltammetric and coulometric measurements were performed on EG&G equipment (potentiostat/galvanostat model 273A). Positive ion ESI mass spectra were obtained in CH_3CN with a Finnigan MAT 95 spectrometer in the range of m/z = 100−1300.

Preparation of Complexes. Solution A. To a suspension of 0.46 g (1 mmol) of $LCrBr_3$[11] in 30 mL methanol was added 0.62 g (2.8 mmol) of $AgClO_4 \cdot H_2O$ with stirring. The suspension was refluxed under argon for 0.5 h yielding a blue-violet solution of $[LCr^{III}(CH_3OH)_3]^{3+}$ with concomitant formation of AgBr. The precipitated AgBr was filtered off, and the clear blue-violet solution A was stored under an argon atmosphere and used for subsequent syntheses.

$[LCr^{III}(PyA)_3Cr^{II}](ClO_4)_2$ (1). To a degassed solution of 25 mL of methanol containing 0.36 g (3 mmol) of *syn*-pyridine-2-aldoxime was added a sample of 0.12 g (1 mmol) of chromium(II) chloride and 0.5 mL of triethylamine with stirring. The solution A was added, and the resulting solution was stirred for 1 h at ambient temperature. After addition of 0.25 g (2 mmol) of $NaClO_4 \cdot H_2O$, the volume of the solution was reduced by passing argon over the surface of the solution. The orange-red microcrystalline product was collected by filtration. Yield: 0.35 g (41%). Anal. Calcd for $C_{27}H_{36}N_9O_{11}Cr_2Cl_2$: C, 38.72; H, 4.33; N, 15.05; Cr, 12.42; ClO_4, 23.64. Found: C, 38.41; H, 4.26; N, 14.95; Cr, 11.98; ClO_4, 23.48. IR (KBr, cm^{-1}): ν(CN) 1638, ν(NO) 1004, ν(pyridine) 1604, 1540, 1475, 1438. UV−vis in CH_3CN [λ_{max}, nm (ϵ, M^{-1} m^{-1})]: 245 (25 540), 302 (23 050), 415 (3570), 517 sh (1760), 910 (140), 1056 (90). ESI-MS (*m*/*z*): 737, 319.

$[LCr^{III}(PyA)_3M^{II}](ClO_4)_2$ (2) (M^{II} = Mn (2), Fe (3), Ni (4), Cu (5), Zn (6)). As complexes **2**−**6** were prepared in a very similar way, a representative method only is described. An argon-scrubbed solution of *syn*-pyridine-2-aldoxime (0.36 g, 3 mmol) in methanol (25 mL) was stirred with $M(ClO_4)_2 \cdot H_2O$ (1 mmol) and triethylamine (0.5 mL) for 0.5 h under argon. The resulting solution was added to the solution A, and the mixture was refluxed for 1 h under argon. The volume of the solution was reduced by passing argon over the surface of the solution until the crystals separated out. The crystals were collected by filtration and air-dried.

The cobalt(III)-containing compound **7**, $[LCr^{III}(pyA)_3Co^{III}](ClO_4)_3$, was obtained by the same procedure using $Co(ClO_4)_2 \cdot 6H_2O$ and air as oxidizing agent.

Complex 2. Yield: 0.39 g (47%). Anal. Calcd for $C_{27}H_{36}N_9CrMnO_{11}Cl_2$: C, 38.58; H, 4.32; N, 15.00; Cr, 6.19; Mn, 6.54; ClO_4, 23.57. Found: C, 38.48; H, 4.22; N, 14.89; Cr, 6.15; Mn, 6.45; ClO_4, 23.08. IR (KBr, cm^{-1}): ν(CN) 1637, ν(NO) 1006, ν(pyridine) 1602, 1550, 1479, 1437. UV−vis in CH_3CN [λ_{max}, nm (ϵ, M^{-1} cm^{-1})]: 263 (22 100), 305 (16 800), 328 sh (9300), 421 (764), 509 sh (460), 690 (30). ESI-MS (*m*/*z*): 740, 320.5.

Complex 3. Yield: 0.35 g (42%). Anal. Calcd for $C_{27}H_{36}N_9CrFeO_{11}Cl_2$: C, 38.54; H, 4.31; N, 14.98; Cr, 6.18; Fe, 6.64; ClO_4, 23.53. Found: C, 38.32; H, 4.04; N, 14.13; Cr, 5.65; Fe, 6.52; ClO_4, 23.25. IR (KBr, cm^{-1}): ν(CN) 1636, ν(NO) 1006, ν(pyridine) 1607, 1555, 1481, 1439. UV−vis in CH_3CN [λ_{max}, nm (ϵ, M^{-1} cm^{-1})]: 211 (38 500), 249 (22 700), 291 (19 300), 522 (8710). ESI-MS (*m*/*z*): 741, 321.

Complex 4. Yield: 0.42 g (50%). Anal. Calcd for $C_{27}H_{36}N_9CrNiO_{11}Cl_2$: C, 38.41; H, 4.30; N, 14.93; Cr, 6.16; Ni, 6.95; ClO_4, 23.52. Found: C, 38.21; H, 4.41; N, 14.76; Cr, 5.77; Ni, 6.71; ClO_4, 23.15. IR (KBr, cm^{-1}): ν(CN) 1634, ν(NO) 1006, ν(pyridine) 1605, 1552,

(6) Parks, J. E.; Wagner, B. E.; Holm, R. H. *Inorg. Chem.* **1971**, *10*, 2472.
(7) Churchill, M. R.; Reis, A. H. *Inorg. Chem.* **1972**, *11*, 1811.
(8) (a) Martin, R. L. In *New Pathways in Inorganic Chemistry*; Ebsworth, Maddock, Sharke, Eds.; Cambridge University Press: Cambridge, U.K., 1968; Chapter 9. (b) Ginsberg, A. P. *Inorg. Chim. Acta Rev.* **1971**, *5*, 45.
(9) (a) Pei, Y.; Journaux, Y.; Kahn, O. *Inorg. Chem.* **1989**, *28*, 100. (b) Mitsumi, M.; Okawa, H.; Sakiyama, H.; Ohba, M.; Matsumoto, N.; Kurisaki, T.; Wakita, H. *J. Chem. Soc., Dalton Trans.* **1993**, 2991. (c) Mallah, T.; Auberger, C.; Verdagner, M.; Veillet, P. *J. Chem. Soc., Chem. Commun.* **1995**, 61. (d) Ohba, M.; Tamaki, H.; Matsumoto, N.; Okawa, H. *Inorg. Chem.* **1993**, *32*, 5385. (e) Gadet, V.; Mallah, T.; Castro, I.; Verdaguer, M.; Veillet, P. *J. Am. Chem. Soc.* **1992**, *114*, 9213. (f) Ohba, M.; Usuki, N.; Fukita, N.; Okawa, H. *Inorg. Chem.* **1998**, *37*, 3349. (g) Berseth, P. A.; Sokol, J. J.; Shores, M. P.; Heinrich, J. L.; Long, J. R. *J. Am. Chem. Soc.* **2000**, *122*, 9655.
(10) Corbin, K. M.; Glerup, J.; Hodgson, D. J.; Lynn, M. H.; Michelsen, K.; Nielsen, K. M. *Inorg. Chem.* **1993**, *32*, 18.
(11) Chaudhuri, P.; Winter, M.; Küppers, H. J.; Wieghardt, K.; Nuber, B.; Weiss, J. *Inorg. Chem.* **1987**, *26*, 3302.
(12) Hartkamp, H. *Z. Anal. Chem.* **1964**, *199*, 183.

Table 1. Crystallographic Data for $[LCr^{III}(PyA)_3Mn^{II}](ClO_4)_2$ (**2**), $[LCr^{III}(PyA)_3Fe^{II}](ClO_4)_2$ (**3**), and $[LCr^{III}(PyA)_3Cu^{II}](ClO_4)_2$ (**5**)

	$Cr^{III}Mn^{II}$ (**2**)	$Cr^{III}Fe^{II}$ (**3**)	$Cr^{III}Cu^{II}$ (**5**)
formula	$C_{27}H_{36}N_9O_{11}Cl_2CrMn$	$C_{27}H_{36}N_9O_{11}Cl_2CrFe$	$C_{27}H_{36}N_9O_{11}Cl_2CrCu$
fw	840.49	841.40	849.09
space group	$P\bar{1}$	$P\bar{1}$	$P\bar{1}$
a (Å)	12.010(2)	12.078(3)	12.063(2)
b (Å)	12.680(3)	12.380(3)	12.627(3)
c (Å)	12.763(3)	12.708(3)	12.910(3)
α (deg)	110.63(3)	99.80(3)	111.74(3)
β (deg)	101.48(3)	99.94(3)	102.04(3)
γ (deg)	101.17(3)	113.27(3)	101.77(3)
V (Å^3)	1707.3(0)	1667.3(7)	1698.7(2)
Z	2	2	2
ρ_{calc} (g cm^{-1})	1.635	1.676	1.666
T (K)	100(2)	100(2)	100(2)
diffractometer[a]	Siemens SMART	Siemens SMART	Siemens SMART
μ (mm^{-1})	0.916	0.995	1.176
no. of indpt reflcns ($F > 4.0\sigma(F)$)	4824	11 166	4793
no. of params	463	463	460
R_F[b] ($F > 4\sigma(F)$)	4.03	4.63	5.88

[a] λ(Mo Kα) = 0.710 73 Å. [b] $R_F = \Sigma(|F_o| - |F_c|)/\Sigma|F_c|$.

Table 2. Crystallographic Data for $[LCr^{III}(PyA)_3Ni^{II}](ClO_4)_2{\cdot}CH_3OH$ (**4**), $[LCr^{III}(PyA)_3Co^{III}](ClO_4)_3$ (**7**), and $[LCr^{III}(P(pyA)_3)Ni^{II}](ClO_4)_2{\cdot}H_2O$ (**8**)

	$Cr^{III}Ni^{II}$ (**4**)	$Cr^{III}Co^{III}$ (**7**)	$Cr^{III}Ni^{II}$ (**8**)
formula	$C_{28}H_{40}N_9O_{12}Cl_2CrNi$	$C_{27}H_{38}N_9O_{16}Cl_3CrCo$	$C_{27}H_{35}N_9O_{11}Cl_2PCrNi$
fw	876.30	961.94	890.22
space group	$C2/c$	$P\bar{1}$	$P\bar{1}$
a (Å)	19.959(4)	10.864(3)	11.989(1)
b (Å)	24.313(5)	12.794(4)	12.429(2)
c (Å)	14.889(3)	14.378(4)	13.292(2)
α (deg)	90	96.03(2)	102.55(2)
β (deg)	93.34(3)	103.62(2)	107.54(3)
γ (deg)	90	96.48(2)	104.00(2)
V (Å^3)	7213(3)	1911.8(10)	1698.7(2)
Z	8	2	2
ρ_{calc} (g cm^{-1})	1.614	1.671	1.699
T (K)	100(2)	293(2)	100(2)
diffractometer[a]	Siemens SMART	Siemens R3m/V	Siemens SMART
μ (mm^{-1})	1.045	1.010	1.128
no of indpt reflcns ($F > 4.0\sigma(F)$)	6315	7553	9114
no. of params	534	518	487
R_F[b] ($F > 4\sigma(F)$)	6.02	5.53	4.17

[a] **λ(Mo Kα)** = 0.710 73 Å. [b] $R_F = \Sigma(|F_o| - |F_c|)/\Sigma|F_c|$.

1476, 1444. UV−vis in CH_3CN [λ_{max}, nm (ϵ, M^{-1} cm^{-1})]: 214 (33 100), 278 (32 200), 304 (29 600), 437 (784), 527 (520), 696 (20), 870 (42). ESI-MS (*m*/*z*): 743, 322.5.

Complex 5. Yield: 0.33 g (39%). Anal. Calcd for $C_{27}H_{36}N_9CrCuO_{11}Cl_2$: C, 38.19; H, 4.27; N, 14.85; Cr, 6.12; Cu, 7.48; ClO_4, 23.32. Found: C, 37.98; H, 4.17; N, 14.67; Cr, 5.88; Cu, 7.65; ClO_4, 23.64. IR (KBr, cm^{-1}): ν(CN) 1636, ν(NO) 1004, ν(pyridine) 1605, 1555, 1478, 1444. UV−vis in CH_3CN [λ_{max}, nm (ϵ, M^{-1} cm^{-1})]: 207 (31 300), 248 (30 500), 301 (26 200), 421 sh (510), 527 (240), 702 (80), 1216 (40). ESI-MS: 748, 324.5.

Complex 6. Yield: 0.42 g (49%). Anal. Calcd for $C_{27}H_{36}N_9CrZnO_{11}Cl_2$: C, 38.11; H, 4.26; N, 14.81; Cr, 6.10; ClO_4, 23.26. Found: C, 38.25; H, 4.28; N, 14.45; Cr, 5.88, ClO_4, 23.45. IR (KBr, cm^{-1}): ν(CN) 1636, ν(NO) 1006, ν(pyridine) 1607, 1555, 1481, 1439. UV−vis in CH_3CN [λ_{max}, nm (ϵ, M^{-1} cm^{-1})]: 258 (25 500), 300 (23 000), 430 (510), 512 (302), 700 sh (80). ESI-MS: 751, 325.

Complex 7. Yield: 0.39 g (41%). Anal. Calcd for $C_{27}H_{36}N_9CrCoO_{15}Cl_3$ (943.47): C, 34.36; H, 3.84; N, 13.35; Cr, 6.16; Co, 6.98; ClO_4, 31.48. Found: C, 34.04; H, 3.16; N, 12.96; Cr, 5.58; Co, 7.10; ClO_4, 31.24. IR (KBr, cm^{-1}): ν(CN) 1635, ν(NO) 1014, ν(pyridine) 1609, 1555, 1474, 1438. UV−vis in CH_3CN [λ_{max}, nm (ϵ, M^{-1} cm^{-1})]: 235 (30 100), 301 (27 300), sh 536 (4240). ESI-MS (*m*/*z*): 843, 744.

$[LCr^{III}(P(PyA)_3)Ni^{II}](ClO4)_2{\cdot}H_2O$ (8). To an argon-scrubbed solution of tris(2-aldoximato-6-pyridyl)phosphine[6] (0.39 g, 1 mmol) and triethylamine (0.5 mL) in methanol (25 mL) was added a solid sample of $Ni(ClO_4)_2{\cdot}6H_2O$ (0.36 g, 1 mmol). After the solution was stirred for 0.5 h, it was added to the solution A and the resulting solution was refluxed for 2 h, whereupon a light red microcrystalline solid precipitated out. The red precipitate was filtered off and recrystallized from methanol/acetonitrile to obtain X-ray-quality crystals. Yield: 0.25 g (29%). Anal. Calcd for $C_{27}H_{35}N_9CrNiO_{11}Cl_2P$: C, 37.18; H, 3.81; N, 14.45; Cr, 5.96; Ni, 6.73; ClO_4, 22.70. Found: C, 37.25; H, 3.89; N, 14.36; Cr, 5.79; Ni, 6.51; ClO_4, 22.49. IR (KBr, cm^{-1}): ν(CN) 1643, ν(NO) 1013, ν(pyridine) 1604, 1527, 1474, 1436. UV−vis in CH_3CN [λ_{max}, nm (ϵ, M^{-1} cm^{-1})]: 258 (24 500), 296 sh (15 880), 433 (820), 520 (380), 921 (57), 974 (60). ESI-MS (*m*/*z*): 771.

Caution! Although we experienced no difficulties with the compounds isolated as their perchlorate salts, the unpredictable behavior of perchlorate salts necessitates extreme caution in their handling.

X-ray Crystal Structure Determinations. The crystallographic data of **2**−**5**, **7**, and **8** are summarized in Tables 1 and 2. Graphite-monochromated Mo Kα X-radiation was used throughout. Intensity data collected at 100 K for all except **7** (at 293 K) were corrected for Lorentz polarization and for absorption effects for **2**−**5** using the program SADABS (G. M. Sheldrick, Universität Göttingen). Absorption correction (Ψ scan) was done in the usual manner for **7**. The structures were solved by direct methods by using the Siemens SHELXTL-PLUS package (G. M. Sheldrick, Universität Göttingen). The function minimized during full-matrix least-squares refinement was $\Sigma w(|F_o| - |F_c|)^2$. Neutral atom scattering factors and anomalous dispersion corrections for non-hydrogen atoms were taken from ref 13. The hydrogen atoms were placed at calculated positions with isotropic thermal parameters;

the methyl groups were treated as rigid bodies. All non-hydrogen atoms were refined with anisotropic thermal parameters.

Results and Discussion

Preparation. The inertness of trivalent chromium ion resulting from a d^3 electron configuration and its high thermodynamic stability with the macrocycle 1,4,7-trimethyl-1,4,7-triazacyclononane together with the lability of the first transition series divalent metal ions are utilized to synthesize $Cr^{III}M^{II}$ binuclear complexes. Practically no scrambling was observed probably because the reaction temperature was too low to surmount the activation barrier to dissociation. It is interesting to note that it was not necessary to isolate the intermediates for this synthetic route.

Although the presence of the $Cr^{III}Co^{II}$ species was observed unequivocally in the mass spectra, all attempts to isolate the species even under strict anaerobic conditions were in vain, presumably because of its strong reducing property, as is evidenced by the electrochemical measurements.

The color of the heterometal dinuclear complexes is light to deep red-brown and is dominated by the $Cr^{III}N_3O_3$ chromophore. They are completely air-stable in the solid state and also in solution at least for a few days.

Since the relevant bands in the IR spectra of comparable oxime-containing heteronuclear complexes have been described earlier[14] and the spectra of complexes **1**−**7** are also very similar, we are refraining from discussing them in details. The bands together with their tentative assignments are given in the Experimental Section.

The electronic spectral results indicate that the complexes **1**−**8** are stable and retain their discrete dinuclear entities also in acetonitrile solution. All dinuclear complexes with the exception of Fe(II)/Co(III)-containing complexes, **3** and **7**, exhibit the lowest energy spin-allowed transition at the Cr(III) center. It allows us to approximate the splitting parameter 10 *Dq* to lie between 19 010 and 19 560 cm^{-1}, which is in agreement with those of the comparable CrN_3O_3 chromophores.[15,16] Interestingly, the second spin-allowed transitions $^4A_2(F) \rightarrow {}^4T_1(F)$ are observed at 421 nm for **2**, 437 for **4**, 421 nm (sh) for **5**, 430 nm for **6**, and 433 nm for **8** with the extinction coefficients ranging from 510 to 820 M^{-1} cm^{-1}. The extinction coefficient of this band is rather large in comparison to those reported for mononuclear $LCrX_3$ complexes. This is probably due to intensity gain via exchange coupling and of the strong trigonal distortion of the Cr(III) geometry, resulting in a lowering of the symmetry to C_3.[17,18] Complex **6**, $Cr^{III}Zn^{II}$, exhibits an additional weak shoulder at 700 nm with $\epsilon_M \sim 80$ M^{-1} cm^{-1} assigned to the spin-forbidden $^4A_2 \rightarrow {}^2E$ transition.

The Cr(III)-centered d−d transitions are missing for the low-spin d^6 systems, **3** and **7**. On the basis of high extinction coefficients and similar $M \rightarrow \pi^*$(oxime) transitions reported in the literature, the peak at 522 nm for **3** and the shoulder at ∼536 nm for **7** can be assigned to the MLCT transitions indicating the strong interactions of the filled t_{2g} orbital with the conjugated π-system of the oxime.[19]

Table 3. Cyclic Voltammetric Data[a]

complex	$E_{1/2}^{ox}$ vs Fc^+/Fc		$E_{1/2}^{red}$ vs Fc^+/Fc	
2, $Cr^{III}Mn^{II}$		+0.71 (qr)		
3, $Cr^{III}Fe^{II}$		+0.61 (r)		
4, $Cr^{III}Ni^{II}$	+1.35 (qr)	+0.90 (r)		
5, $Cr^{III}Cu^{II}$				−0.73 (r)
6, $Cr^{III}Zn^{II}$				−1.83 (r)
7, $Cr^{III}Co^{III}$			−0.52 (r)	−1.36 (r)
8, $Cr^{III}Ni^{II}P(PyA)_3$		+0.90 (r)		

[a] r = reversible; qr = quasi-reversible.

Judged on the basis of extinction coefficients, the bands at 910 and 1056 nm for **1** (Cr^{II}), 690 nm for **2** (Mn^{II}), 696 and 870 nm for **4** (Ni^{II}), 702 and 1216 nm for **5** (Cu^{II}), and 920 and 974 nm for **8** (Ni^{II}) are tentatively ascribed to the d−d transitions at the M(II) center.

Electrospray-Ionization Mass Spectrometry (ESI-MS). ESI-MS in the positive mode has been proved to be a very useful analytical tool for characterization of complexes **1**−**8**. Major peaks are listed in the Experimental Section. Shown in Figure S1 (Supporting Information) is the positive ion ESI mass spectrum in CH_3CN of **6**, $[LCr(PyA)_3Zn](ClO_4)_2$, showing that there are only two peaks at *m*/*z* 751 and 325 corresponding to the monocation $[LCr(PyA)_3Zn(ClO_4)]^+$ and the dication $[LCr(PyA)_3Zn]^{2+}$, respectively. The ESI-MS results for other $[LCr(PyA)_3M^{II}](ClO_4)_2$ **1**−**5** are very similar to that of **6**. Interestingly, all complexes **1**−**6** show the doubly charged species $[LCr(PyA)_3M^{II}]^{2+}$ as the base peak (100%). On the other hand, the base peaks for **7** and **8** are observed at *m*/*z* 843 and 771, corresponding to the monocharged $[LCr(PyA)_3Co(ClO_4)_2]^+$ and $[LCrP(PyA)_3Ni(ClO_4)]^+$ species. There is practically no indication in the spectra for ligand fragmentation or cleavage of the dimer evidencing the robustness of the clathrochelates derived from the pyridinealdoxime and the chromium-containing capping agent. The insets in Figure S1 (Supporting Information) illustrate that the resolution is sufficient to determine the formal charge of the complex cations and provide a check on the isotopic patterns. To conclude, the data summarized in the Experimental Section and in Figure S1 show that mass spectrometry of the complexes unambiguously demonstrates the nuclearity of all complexes examined and also provides identification of the metal centers and the composition of the complexes. It seems that complexes **1**−**8** are not fragile and can withstand the conditions of the ESI(pos)-MS ionization.[20]

Electrochemistry. The cyclic voltammograms (CV) of complexes **2**−**8** were measured at ambient temperature in CH_3CN containing 0.1 M tetra-*n*-butylammonium hexafluorophosphate as supporting electrolyte at a glassy carbon working electrode. The results are summarized in Table 3 and Figure S2 (Supporting Information). All redox potentials are referenced in volts versus the ferrocenium/ferrocene couple (Fc^+/Fc), used as an internal standard to be 0.09 V vs $Ag/AgNO_3$.

Two irreversible electron-transfer waves, $E_p^{ox} \sim +1.30$ V and $E_p^{red} \sim -1.8$ V are detected in the potential range +1.8 to −2.0 V for most of the complexes. We assign the oxidation process to the ligand pyridine-2-aldoxime, rather than the Cr(III)- or M-centered electron-transfer, on the basis of the fact that for analogous complexes $Co^{III}M$, $Fe^{III}M$, and $Mn^{III}M$ similar ligand oxidations have been observed at comparable potentials (1.1−1.3 V).[21] High peak current of E_p^{ox} observed

(13) *International Tables for X-ray Crystallography*; Kynoch: Birmingham, England, 1974; Vol. 4.
(14) Birkelbach, F.; Winter, M.; Flörke, U.; Haupt, H.-J.; Butzlaff, C.; Lengen, M.; Bill, E.; Trautwein, A. X.; Wieghardt, K.; Chaudhuri, P. *Inorg. Chem.* **1994**, *33*, 3990.
(15) Caldwell, S. H.; House, D. A. *J. Inorg. Nucl. Chem.* **1969**, *31*, 811.
(16) Wieghardt, K.; Chaudhuri, P.; Nuber, B.; Weiss, J. *Inorg. Chem.* **1982**, *21*, 3086.
(17) Lever, A. B. P. *Inorganic Electronic Spectroscopy*; Elsevier: Amsterdam, 1984.
(18) McCarthy, P. J.; Güdel, H. U. *Coord. Chem. Rev.* **1988**, *88*, 69.
(19) Krumholz, P. *Struct. Bonding (Berlin)* **1971**, *9*, 139.
(20) Budzikiewicz, H. *Mass Spectrometry*; Wiley-VCH: Weinheim, New York, 1998.
(21) Ross, S. Dissertation, Bochum, Germany, 1998.

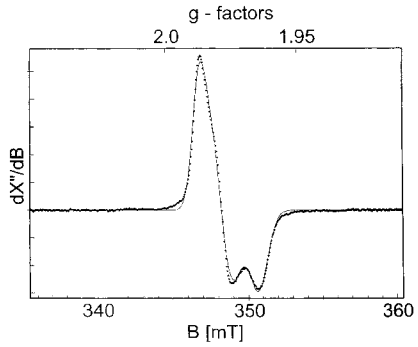

Figure 1. X-band EPR spectrum (···) and its simulation (—) of the electrochemically oxidized complex **6**, $Cr^{III}Zn^{II}$, in CH_3CN at 10 K (microwave frequency 9.65 GHz; power 100.6 μW; modulation amplitude 11.4 G).

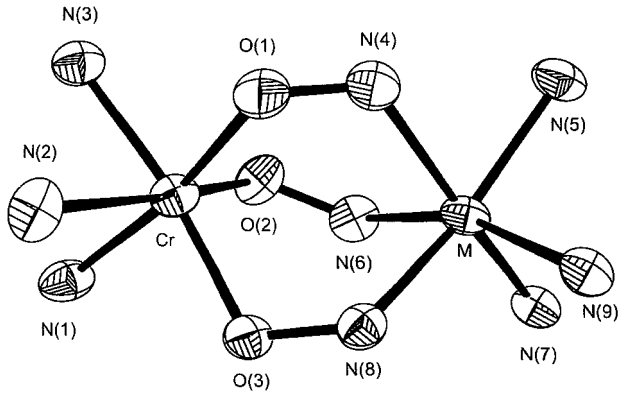

Figure 2. First coordination sphere of **2**. The atom connectivities are identical for **3**−**5**, **7**, and **8**.

for **6**, $Cr^{III}Zn^{II}$, is in line with the notion of ligand oxidation. Similar irreversible oxidation of pyridine-2-aldoxime in its Ni(II) complexes at potentials >1 V has been described in the literature.[22] That the oxidation process is ligand-centered is also indicated by EPR measurements of the two-electron oxidized product, generated electrochemically from **6**, $Cr^{III}Zn^{II}$. The two-electron-oxidized species (two ligand radicals presumably based on oximes) is readily prepared electrochemically in solution by coulometry at an appropriately fixed potential at −25 °C. The species is stable at low-temperature for a few days and amenable to characterization spectroscopically by EPR measurements at 10 K (Figure 1). An EPR spectrum with $g_x = 1.99$, $g_y = 1.98$, and $g_z = 1.97$ ($S = 1/2$) for the oxidized **6** is in accord with a spin-coupling model involving antiferromagnetic exchange coupling between two oxime-based radicals ($2 \times S = 1/2$) due to ligand oxidation and the Cr(III) center ($S = 3/2$). We realize that the EPR spectrum can also be interpreted as arising from a d^1 system (Cr^V) or an exchange-coupled $d^2(Cr^{IV})$−ligand radical system. The EPR spectrum of **6** with signals at $g \approx 1.97$ and 3.88 is in full conformity with an $S = 3/2$ system arising from Cr(III) in **6**, $Cr^{III}Zn^{II}$ (Figure 5).

Interestingly, the reduction at −1.83 V of **6**, $Cr^{III}Zn$, is reversible and assigned also to the pyridinealdoxime-centered reduction on the basis of the observation that analogous isostructural $Co^{III}Zn^{II}$ compound exhibits three reversible one-electron-transfer waves at −0.20 V (Co^{III}/Co^{II}), −1.07 V (Co^{II}/Co^{I}), and −1.83 V (PyA/PyA-radical anion). This ligand-centered reduction is not observed for $Cr^{III}Co^{III}$ (**7**) and $Cr^{III}Cu^{II}$ (**5**). Two reversible one-electron-transfer waves are detectable at $E_{1/2}^{red1} = -0.52$ V and $E_{1/2}^{red2} = -1.36$ V for **7,** $Cr^{III}Co^{III}$, and one reversible reduction is detectable at $E_{1/2}^{red} = -0.73$ V for **5,** $Cr^{III}Cu^{II}$, which can be assigned to the following equilibria:

$$Cr^{III}Co^{III} \overset{E_{1/2}^{red1}}{\rightleftharpoons} Cr^{III}Co^{II} \overset{E_{1/2}^{red2}}{\rightleftharpoons} Cr^{III}Co^{I}$$

$$Cr^{III}Cu^{II} \overset{E_{1/2}^{red}}{\rightleftharpoons} Cr^{III}Cu^{I}$$

The cyclic voltammetric behaviors of $Cr^{III}M^{II}$ (M = Mn (**2**), Fe (**3**), Ni (**4**), $NiP(PyA)_3$ (**8**)) show in each case one reversible one-electron oxidation at +0.71, +0.61, and +0.90 V, which are assigned to the M-centered oxidations resulting in the couples Mn(III)/Mn(II) for **2**, Fe(III)/Fe(II) for **3**, and Ni(III)/Ni(II) for **4** and **8**. It is noteworthy, in contrast to the stabilization of Ni(IV) generally by oxime ligands,[23] no stabilization of the Ni(IV) state in **4** and **8** by the ligand pyridine-2-aldoxime has been observed. A similar observation of the ability of pyridine-2-aldoxime to stabilize Ni(III), but not Ni(IV), has been reported earlier.[24]

Mössbauer Parameters of 3. The Mössbauer spectrum of $[LCr(PyA)_3Fe^{II}](ClO_4)_2$, **3**, was measured at 80 K in zero-field to determine the spin and oxidation state of the iron center. The Mössbauer parameters of **3** ($\delta = 0.25$ mm/s, $\Delta E_Q = 0.35$ mm/s) clearly indicate the low-spin nature of the Fe(II) ion, as is also indicated by the structural data. The slight asymmetry in the ligand field of the iron center is reflected also in the quadrupole splitting.[25]

Molecular Structures of $[LCr^{III}(PyA)_3M^{II}](ClO_4)_2$ (M = Mn (2), Fe (3), Ni (4), Cu (5)), $[LCr^{II}(PyA)_3Co^{III}](ClO_4)_3$ (7), and $[LCr^{III}\{P(PyA)_3\}Ni^{II}](ClO_4)_2$ (8). The X-ray structures confirm that mixed-metal $Cr^{III}M^{II}$ and $Cr^{III}Co^{III}$ complexes have indeed been formed with a geometry in which two pseudooctahedral polyhedra are joined by three oximato N−O groups. The coordinated ligand L exhibits no unexpected features.[26] The N−O (average 1.351 ± 0.015 Å) and C=N_{ox} (average 1.288 ± 0.010 Å) bond lengths and C−N−O bond angle (average 118.2 ± 1.6°) of the bridging pyridinealdoximate ligand are found to be very similar to those of other comparable structures.[27] Figure 2 illustrates the thermal ellipsoid drawing of the $N_3Cr(O-N)_3M(N_{py})_3$ core for the $Cr^{III}Mn^{II}$ compound, **2**. Following the atom-numbering scheme depicted in Figure 2, Table 4 lists bond lengths of the first coordination sphere of the $Cr^{III}M$ compounds, **2**−**5**, **7**, and **8**. For comparison purpose important structural parameters are given in Table 5. As expected, the donor atoms for the metal ions of the cations in **2**−**5**, **7**, and **8** are identical, CrN_3O_3 and $M(N_{py})_3(N_{ox})_3$, but not the coordination geometry of the divalent metal centers and of trivalent Co(III). Perspective views of the cations for only **2**, **4**, **5**, and **8** are shown in Figure 3.

The chromium coordination geometry is distorted octahedral with three nitrogen atoms, N(1), N(2), and N(3), from the

(22) Orama, M.; Saarinen, H.; Korvenranta, J. *Acta Chem. Scand.* **1989**, *43*, 407.

(23) (a) Chakravorty, A. *Isr. J. Chem.* **1985**, *25*, 99. (b) Nag, K.; Chakravorty, A. *Coord. Chem. Rev.* **1980**, *33*, 87.

(24) Drago, R. S.; Baucom, E. I. *Inorg. Chem.* **1972**, *11*, 2064.

(25) (a) Gütlich, P.; Link, R.; Trautwein, A. X. *Mössbauer Spectroscopy and Transition Metal Chemistry*; Springer-Verlag: Berlin, Heidelberg, New York, 1978. (b) Gütlich, P. In *Mössbauer Spectroscopy*; Gonser, U., Ed.; Springer-Verlag: Berlin, 1975; Chapter 2.

(26) Chaudhuri, P.; Wieghardt, K. *Prog. Inorg. Chem.* **1987**, *35*, 329.

(27) (a) Beckett, R.; Hoskins, B. F. *J. Chem. Soc., Dalton Trans.* **1972**, *291*, 2527. (b) Nasakkala, M.; Saarinen, H.; Korvenranta, J.; Orama, M. *Acta Crystallogr.* **1989**, *C45*, 1514. (c) Pearse, G. A.; Raithby, P. R.; Lewis, J. *Polyhedron* **1989**, *8*, 301. (d) Schlemper, E. O.; Stunkel, J.; Patterson, C. *Acta Crystallogr.* **1990**, *C46*, 1226. (e) Nordquest, K. W.; Phelps, D. W.; Little, W. F.; Hodgson, D. J. *J. Am. Chem. Soc.* **1976**, *98*, 1104.

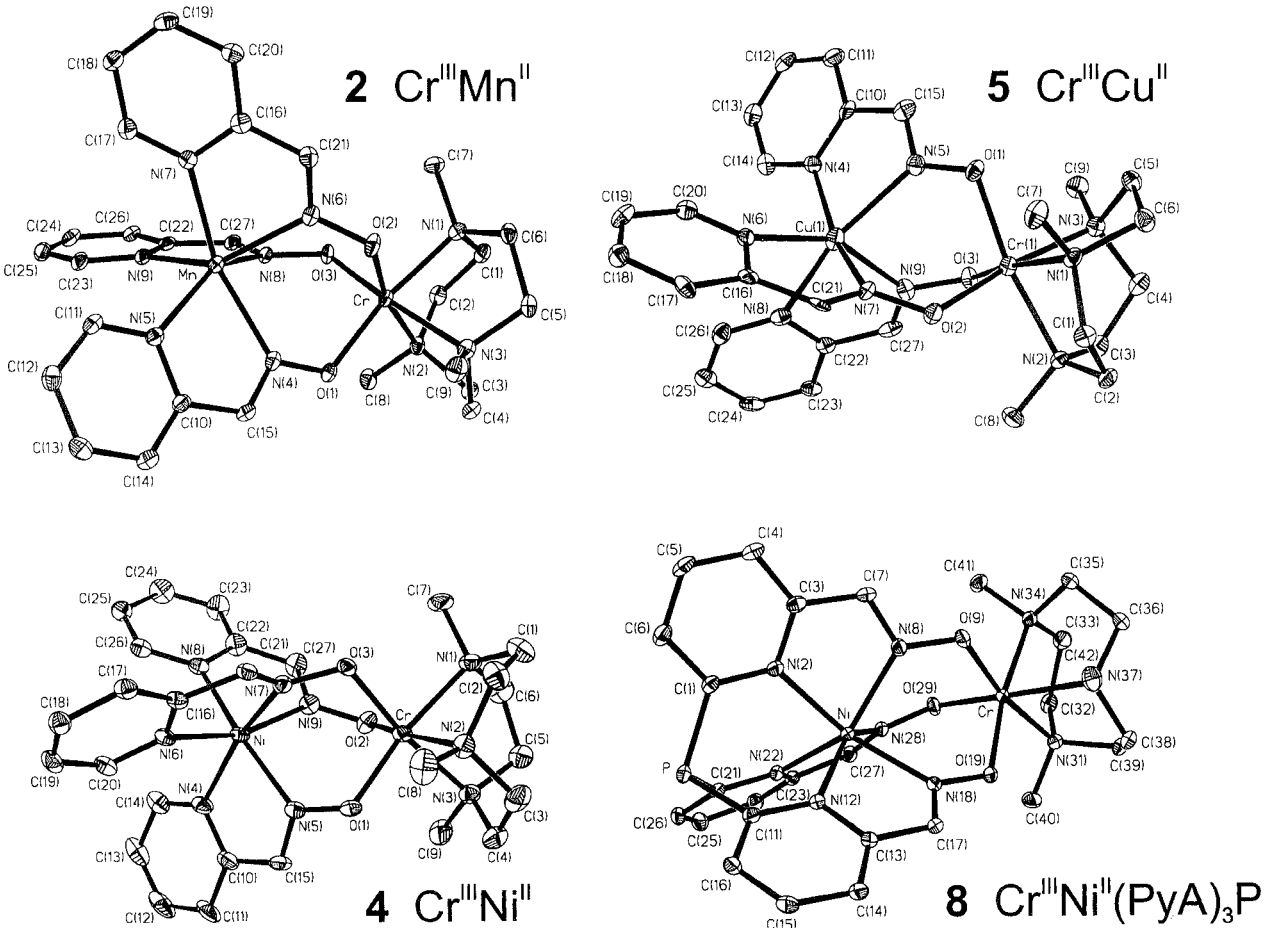

Figure 3. Molecular structures of the dications $Cr^{III}Mn^{II}$ in **2**, $Cr^{III}Ni^{II}$ in **4**, $Cr^{III}Cu^{II}$ in **5**, and $[LCr\{P(PyA)_3\}Ni]^{2+}$ in crystals of **8**. Note the atom-numbering different from that in Figure 2.

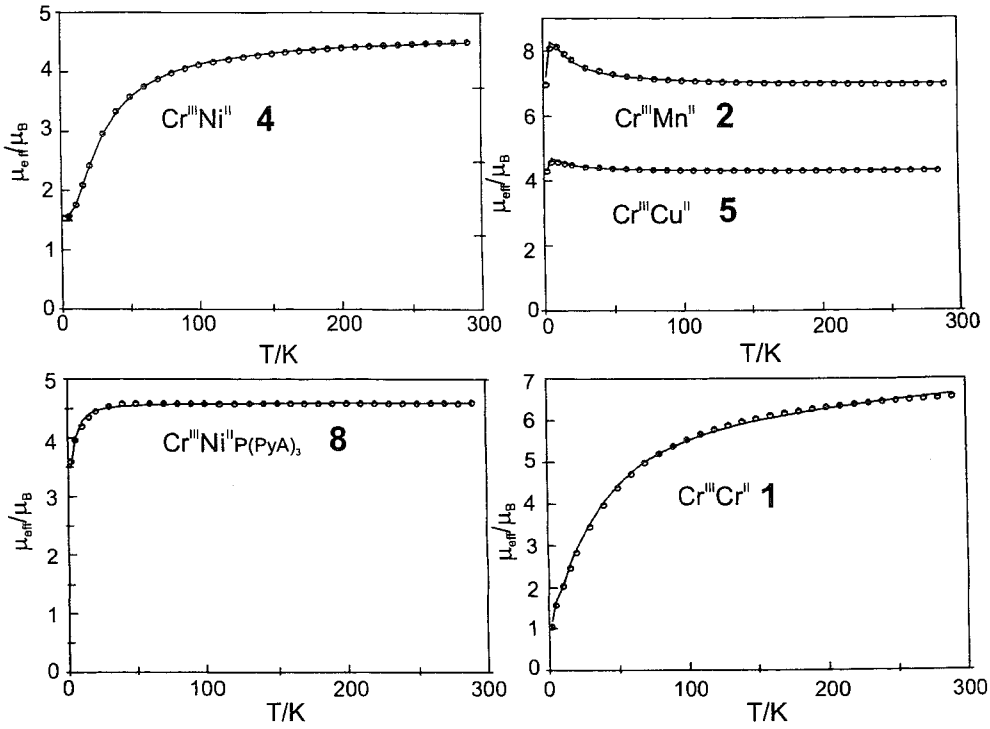

Figure 4. Plots of μ_{eff} vs T for solid **1**, **2**, **4**, **5**, and **8**. The solid lines represent the best fit of the data to the Heisenberg−Dirac−van Vleck model (see text).

facially coordinated tridentate macrocyclic amine L and three oxygen atoms, O(1), O(2), and O(3), from the bridging oximate group (Figure 2). The Cr−N (average 2.106 ± 0.018 Å) and Cr−O (average 1.959 ± 0.015 Å) distances for complexes **2**−**8**

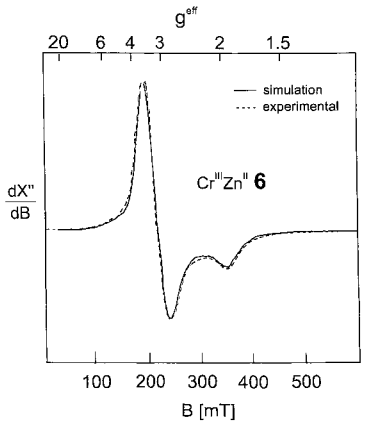

Figure 5. X-band EPR spectrum of **6**, $Cr^{III}Zn^{II}$, in CH_3CN at 4 K (experimental conditions: microwave frequency 9.64 GHz; power 1 mW; modulation amplitude 11.4 G) together with the simulated spectrum.

correspond to the literature values for Cr(III) complexes with this macrocyclic amine.[26,28] Deviations from idealized octahedral geometry are found for the ligand L, the N−Cr−N angles ranging between 82.3(1) and 84.2(2)°, whereas O−Cr−O angles fall between 92.4(1) and 98(1)° for complexes **2**−**8**. The second metal atom, which is separated from the chromium center at a distance of 3.4−3.7 Å, does not affect the geometry of the chromium center in complexes **2**−**8**.

The second metal center, Mn(II), Fe(II), Ni(II), or Co(III), is also 6-fold-coordinated yielding an MN_6 core. Coordination occurs facially through pyridine nitrogen atoms, $N_{py}(5)$, $N_{py}(7)$, and $N_{py}(9)$, and three azomethine nitrogen atoms, $N_{ox}(4)$, $N_{ox}(6)$, and $N_{ox}(8)$, from the pyridinealdoxime (PyA) ligand (Figure 2). It is noteworthy that the $M-N_{ox}$ bond lengths are shorter than the $M-N_{py}$ bond distances: 0.02 Å for Mn^{II} (**2**); 0.06 Å for Fe^{II} (**3**), Ni^{II} (**4**), and Co^{III} (**7**); 0.01 Å for Ni^{II} (**8**). A similar trend was also found for BF-capped mononuclear complexes with the PyA ligand.[7,29] The average $M-N_{py}$ and $M-N_{ox}$ bond lengths fall within the ranges that are considered as normal covalent bonds for M(II) or Co(III) centers with a high-spin configuration for Mn(II) (d^5) (**2**) and Ni(II) (d^8) (**4**, **8**) and a d^6 low-spin electronic configuration for Fe(II) (**3**) and Co(III) (**7**).

The Cu−N distances (Table 4) and the twist angles ϕ (Table 5) show that the resultant coordination sphere around the copper center in **5** is strongly distorted. The geometry of the Cu center may be envisaged as pseudo-trigonal-pyramidal with a non-bonded pyridine N(5) (Figure 2) or N(8) in Figure 3.

A comparison of the two isoelectronic d^3d^8 complexes **4** and **8**, $Cr^{III}Ni^{II}$, shows that the twist angles ϕ and the dihedral angles θ in $[LCr\{P(PyA)_3\}Ni]^{2+}$ (**8**) are indeed smaller than those in **4,** $[LCr(PyA)_3Ni]^{2+}$ (Table 5).

All of the structural data are consistent with the geometrical distortions from octahedron of the metal ions Mn(II), Fe(II), Co(III), Ni(II), and Cu(II) in complexes **2**, **3, 7, 4** and **8**, and **5**, respectively, and the distortions can be ascribed to both of the factors, electronic (LFSE) and size effects, as has been discussed earlier.[28,30]

Magneto−Chemical Studies. Magnetic susceptibility data for polycrystalline samples of complexes **1**−**8** were collected in the temperature range 2−290 K in an applied magnetic field of 1 T to characterize the nature and magnitude of the exchange interaction propagated by the bridging oxime ligands. We use the Heisenberg spin Hamiltonian in the form $H = -2J\hat{S}_{Cr}\hat{S}_M$ for an isotropic exchange coupling with $S_{Cr} = 3/2$ and $S_M = 0$ for Fe(II) (**3**), Zn(II) (**6**), and Co(III) (**7**), $S_M = 2$ for Cr(II) (**1**), $S_M = 5/2$ for Mn(II) (**2**), $S_M = 1$ for Ni(II) (**4** and **8**), and $S_M = 1/2$ for Cu(II) (**5**). The experimental magnetic data were simulated using a least-squares fitting computer program[31] with a full-matrix diagonalization of exchange coupling, Zeeman splitting, and axial single-ion zero-field interactions (DS_z^2), if necessary. The experimental data are displayed in Figures S3 (Supporting Information) and 4 as the effective magnetic moment (μ_{eff}) versus temperature. The solid lines in the Figures S3 and 4 represent the simulations. Table 6 summarizes the intradimer exchange parameter together with the observed spin ground states.

As the complexes **3**, **6**, and **7** containing only one paramagnetic center, viz. Cr(III) ($S_{Cr} = 3/2$), may be considered magnetically as mononuclear complexes, we start our discussion with their magnetic properties. Above $T \approx 20$ K complexes **3**, **6,** and **7** exhibit essentially temperature-independent μ_{eff} values of 3.87 ± 0.01, 3.76 ± 0.04, and 3.81 ± 0.01 μ_B, respectively. There are three unpaired electrons localized on the Cr(III) center in **3**, **6**, and **7**, and the "spin-only" ($g = 2.0$) magnetic moment is 3.87 μ_B. The experimental μ_{eff} values clearly indicate that we are dealing with genuine $Cr^{III}Fe^{II}$(ls) (**3**), $Cr^{III}Zn^{II}$ (**6**), and $Cr^{III}Co^{III}$(ls) (**7**) species with a low-spin diamagnetic d^6 Fe(II) or Co(III) ion and a diamagnetic d^{10} Zn(II) ion, in complete agreement with EPR and Mössbauer results. Simulations of the experimental magnetic moment data yield g_{Cr} values of 1.98 for **3**, 1.96 for **6**, and 1.98 for **7** with $S_{Cr} = 3/2$ and $S_M = 0$ (Figure S3).

The magnetic moment μ_{eff}/molecule for **1**, $Cr^{III}Cr^{II}$ of 6.17 μ_B ($\chi_M T = 4.752$ cm^3 K mol^{-1}) at 290 K decreases monotonically with decreasing temperature until it reaches a value of 0.98 μ_B ($\chi_M T = 0.1188$ cm^3 mol^{-1} K) at 2 K; this temperature dependence of μ_{eff} is a clear indication of an antiferromagnetic exchange coupling between two paramagnetic centers Cr(III) ($S = 3/2$) and Cr(II) ($S = 2$) with a resulting $S_t = 1/2$ ground state. The solid line in Figure 4 represents the best fit with the following parameters: $J = -7.9$ cm^{-1}; $g_{Cr(III)} = 1.98$; $g_{Cr(II)} = 2.05$.

The magnetic behavior of **2**, $Cr^{III}Mn^{II}$, is characteristic of a ferromagnetically coupled dinuclear complex. At 290 K the μ_{eff} value of 6.96 μ_B ($\chi_M T = 6.052$ cm^3 K mol^{-1}) increases monotonically with decreasing temperature until it reaches a maximum at 10 K with $\mu_{eff} = 8.13$ μ_B ($\chi_M T = 8.263$ cm^3 K mol^{-1}). Below 10 K there is a decrease in μ_{eff} reaching a value of 6.96 μ_B ($\chi_M T = 6.064$ cm^3 K mol^{-1}) at 2 K. A least-squares fit, shown as the solid line in Figure 4, with $J = +1.5$ cm^{-1}, $g_{Cr} = 1.99$, and $g_{Mn} = 1.95$ was obtained. We realize that the error associated with a small positive J-value may be large. Irrespective of that, the μ_{eff} vs T plot for **2** (Figure 4) demonstrates unambiguously the ferromagnetic nature of the exchange coupling. Thus, the $Cr^{III}-Mn^{II}$ interaction in **2** is ferromagnetic like comparable systems reported earlier by us.[28]

(28) Burdinski, D.; Birkelbach, F.; Weyhermüller, T.; Flörke, U.; Haupt, H.-J.; Lengen, M.; Trautwein, A. X.; Bill, E.; Wieghardt, K.; Chaudhuri, P. *Inorg. Chem.* **1998**, *37*, 1009.

(29) (a) Churchill, M. R.; Reis, A. H., Jr. *Inorg. Chem.* **1972**, *11*, 2299. (b) Faller, J. W.; Blankenship, C.; Whitmore, B.; Sena, S. *Inorg. Chem.* **1985**, *24*, 4483. (c) Churchill, M. R.; Reis, A. H., Jr. *Inorg. Chem.* **1973**, *12*, 2280.

(30) (a) Wentworth, R. A. D. *Coord. Chem. Rev.* **1972/73**, *9*, 171. (b) Kirchner, R. M.; Meali, C.; Bailey, M.; Howe, N.; Torre, L. P.; Wilson, L. J.; Andrews, L. C.; Rose, N. J.; Lingafelter, E. C. *Coord. Chem. Rev.* **1987**, *77*, 89. (c) Kunow, S. A.; Takeuchi, K. J.; Grzybowski, J. J.; Jircitano, A. J.; Goedken, V. L. *Inorg. Chim. Acta* **1996**, *241*, 21.

(31) Birkelbach, F.; Krebs, C.; Staemmler, V. Unpublished computer program, Bochum, Germany, 1997.

Table 4. Selected Bond Distances (Å) for Complexes $Cr^{III}Mn^{II}$ (**2**), $Cr^{III}Fe^{II}$ (**3**), $Cr^{III}Ni^{II}$ (**4**), $Cr^{III}Cu^{II}$ (**5**), $Cr^{III}Co^{III}$ (**7**), and $Cr^{III}NiP(PyA)_3$ (**8**)

Cr−M	$Cr^{III}Mn^{II}$ (**2**)	$Cr^{III}Fe^{II}$ (**3**)	$Cr^{III}Co^{III}$ (**7**)	$Cr^{III}Ni^{II}$ (**4**)	$Cr^{III}Cu^{II}$ (**5**)	$Cr^{III}NiP(PyA)_3$ (**8**)
Cr−N(1)	2.115(3)	2.112(2)	2.089(4)	2.107(4)	2.112(5)	2.110(2)
Cr−N(2)	2.121(3)	2.103(2)	2.084(4)	2.111(4)	2.113(5)	2.116(2)
Cr−N(3)	2.116(3)	2.104(2)	2.084(4)	2.110(4)	2.105(5)	2.110(2)
Cr−O(1)	1.949(2)	1.962(2)	1.980(3)	1.952(3)	1.955(4)	1.944(2)
Cr−O(2)	1.952(2)	1.961(2)	1.973(3)	1.949(3)	1.960(4)	1.940(2)
Cr−O(3)	1.943(2)	1.962(2)	1.962(3)	1.969(3)	1.958(4)	1.935(2)
$M-N(4)_{ox}$	2.254(3)	1.898(2)	1.896(4)	2.040(4)	2.104(6)	2.103(2)
$M-N(6)_{ox}$	2.231(3)	1.904(2)	1.888(4)	2.042(4)	2.205(6)	2.099(2)
$M-N(8)_{ox}$	2.235(3)	1.910(2)	1.890(4)	2.056(4)	1.983(5)	2.076(2)
$M-N(5)_{py}$	2.258(2)	1.986(2)	1.961(4)	2.115(4)	2.490(6)	2.087(2)
$M-N(7)_{py}$	2.272(3)	1.984(2)	1.965(4)	2.109(4)	2.061(5)	2.104(2)
$M-N(9)_{py}$	2.242(3)	1.970(2)	1.974(4)	2.097(4)	2.054(5)	2.109(2)

Table 5. Important Structural Parameters for Complexes **2**−**5**, **7**, and **8**

complex	$Cr^{III}\cdots M$ (Å)	av twist angle ϕ (deg)[a]	dihedral angle θ (deg)[b]
2, $Cr^{III}Mn^{II}$	3.711	9.8	28.3/30.8/35.2
3, $Cr^{III}Fe^{II}$(ls)	3.386	45.8	40.0/44.6/45.4
4, $Cr^{III}Ni^{II}$	3.510	37.2	37.6/37.6/42.2
5, $Cr^{III}Cu^{II}$	3.558	29.0	25.8/36.4/39.7
7, $Cr^{III}Co^{III}$(ls)	3.415	48.6	43.2/45.9/46.3
8, $Cr^{III}Ni^{II}P(PyA)_3$	3.590	13.6	19.7/21.2/21.5

[a] The trigonal twist angle ϕ is the angle between the triangular faces comprising N(4)N(6)N(8) and N(5)N(7)N(9) and has been calculated as the mean of the Newman projection angles viewed along the centroids of focus. For an ideal trigonal prismatic arrangement, ϕ is 0 and 60° for an octahedron (or trigonal-antiprismatic arrangement). [b] That the core Cr(O−N)M is not linear is shown by the dihedral angles θ between the planes comprising Cr(O−N) and M(N−O) atoms.

Table 6. Magnetic Parameters for Heterodinuclear Complexes **1**−**8**

complex	J (cm^{-1})	g_{Cr}	g_M	ground state (S_t)
1, $Cr^{III}Cr^{II}$	−7.9	1.98	2.05	$S_t = 1/2$
2, $Cr^{III}Mn^{II}$	+1.5	1.99	1.95	$S_t = 8/2$
3, $Cr^{III}Fe^{II}$(ls)		1.98		$S_t = 3/2$
4, $Cr^{III}Ni^{II}$	−9.2	2.0	2.19	$S_t = 1/2$
5, $Cr^{III}Cu^{II}$ [b]	+1.8	1.98	2.08	$S_t = 4/2$
6, $Cr^{III}Zn^{II}$		1.96		$S_t = 3/2$
7, $Cr^{III}Co^{III}$(ls)		1.98		$S_t = 3/2$
8, $Cr^{III}Ni^{II}(PyA)_3P$[a]	0	1.98	2.16	$S_{Cr} = 3/2$, $S_{Ni} = 1$

[a] $\theta = -1.42$ K. [b] $D = 2$ cm^{-1}.

Interestingly, most of the known Cr(III)−Mn(II) interactions in the literature[10,11] are antiferromagnetic in nature.

The experimental magnetic moment of **4**, $Cr^{III}Ni^{II}$, decreases as the temperature is lowered reaching a value of 1.71 μ_B ($\chi_M T = 0.3638$ cm^3 K mol^{-1}) at 7.4 K which is nearly the "spin-only" value of $\mu_{eff} = 1.73$ μ_B for an $S_t = {}^1/_2$ ground state, resulting from the antiferromagnetic interaction between Cr(III) and Ni(II) ions in complex **4**. Below 7 K there is a decrease in μ_{eff} reaching a value of 1.46 μ_B

($\chi_M T = 0.2659$ cm^3 K mol^{-1}) at 2 K. A simulation, shown as the solid line in Figure 4, of the magnetic data yields the following parameters: $J = -9.20$ cm^{-1}; $g_{Cr} = 1.995$; $g_{Ni} = 2.193$. To fit the data point at $T = 2$ K, it was necessary to consider intermolecular interactions (Weiss constant Θ), J, and g_{Ni} as adjustable parameters. $g_{Cr} = 1.98$, evaluated for other complexes, was kept fixed during simulation to avoid overparametrization. Simulated parameters in the latter case, $J = -9.1$ cm^{-1}, $g_{Cr} = 1.98$ (fixed), $g_{Ni} = 2.216$, and $\Theta = -0.23$ K, show that introduction of the Weiss constant Θ has practically no effect on the obtained J value, although the quality of fit slightly increases.

The interaction between the Cr(III) and Ni(II) ions gives rise to $S_t = 5/2$, 3/2, and 1/2 states, with an energy gap of 5J between the sextet−quartet and 3J between the quartet−doublet states. The corresponding Zeeman factors $g_{|5/2>}$, $g_{|3/2>}$, and $g_{|1/2>}$ are related[33−35] to the local Zeeman factors g_{Cr} and g_{Ni}. The following energy diagram appropriate for **4** is obtained from the magnetic studies: The magnetic moment, μ_{eff}, for **5,** $Cr^{III}Cu^{II}$,

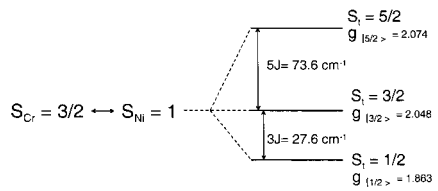

at 290 K is 4.25 μ_B ($\chi_M T = 2.260$ cm^3 K mol^{-1}), which is very close to the theoretical value of $\mu_{eff} = 4.239$ μ_B expected for two uncoupled spins of $S_{Cu} = 1/2$ and $S_{Cr} = 3/2$. On lowering of the temperature, μ_{eff} increases monotonically until a plateau is reached in the temperature range 10−5 K with a μ_{eff} value of 4.53 μ_B ($\chi_M T = 2.57$ cm^3 K mol^{-1}), which is slightly lower than the theoretical "spin-only" value of 4.90 μ_B for $S = 2$, expected as the ground state for a ferromagnetically coupled $Cr^{III}Cu^{II}$ compound. Below 10 K there is a decrease in μ_{eff} reaching a value of 4.26 μ_B ($\chi_M T = 2.265$ cm^3 K mol^{-1}) at 2 K. This deviation from the theoretical value is attributable to the zero-field splitting of the ground-state $S_t = 2$. The least-squares fitting, shown as the solid line in Figure 4, of the experimental data leads to $J = +1.8$ cm^{-1}, $g_{Cr} = 1.98$, $g_{Cu} = 2.08$, and $D_{Cr} = 2.0$ cm^{-1}. To firmly establish the positive sign of the exchange coupling constant, we addressed the point of global and local minima by consideration of the two-dimensional contour projection of the error surface. The error surface shows that the fitting procedure has correctly identified the global minimum, and we conclude that **5** has an $S_t = 2$ ground state lying 7.2 cm^{-1} below the excited-state $S_t = 1$. The fitted g_{Cr} value for **5** is in conformity with the experimentally (susceptibility) obtained g_{Cr} values for **3,** $Cr^{III}Fe^{II}$(ls), and **7,** $Cr^{III}Co^{III}$-(ls). The observed ferromagnetic coupling ($J = +1.8$ cm^{-1}) is the weakest among the reported $Cr^{III}Cu^{II}$ compounds in the literature.[9d,14,32a,36]

The magnetic moment μ_{eff} for **8**, $Cr^{III}Ni^{II}P(pyA)_3$, which is the isoelectronic analogue of **4,** exhibits an essentially temper-

(32) (a) Corbin, K. M.; Glerup, J.; Hodgson, D. J.; Lynn, M. H.; Michelsen, K.; Nielsen, K. M. *Inorg. Chem.* **1993**, *32*, 18. (b) Scuiller, A.; Mallah, T.; Novorozkhin, A.; Thalence, J.-L.; Verdaguer, M.; Veillet, P. *New J. Chem.* **1996**, *20*, 1. (c) Ohba, M.; Usuki, N.; Fukita, N.; Okawa, H. *Angew. Chem., Int. Ed. Engl.* **1999**, *38*, 1795. (d) Marvilliers, A.; Parsons, S.; Riviére, E.; Audiére, J.-P.; Mallah, T. *Chem. Commun.* **1999**, 2217.

(33) (a) Chao, C. C. *J. Magn. Reson.* **1973**, *10*, 1. (b) Scaringe, R. P.; Hodgson, D. J.; Hatfield, W. E. *Mol. Phys.* **1978**, *35*, 701.

(34) Bencini, A.; Gatteschi, D. *EPR of Exchange Coupled Systems*; Springer-Verlag: Berlin, 1990.

(35) Kahn, O. *Molecular Magnetism*; VCH-Verlagsgesellschaft: Weinheim, Germany, 1993.

ature-independent behavior in the range 290−30 K with $\mu_{eff} = 4.85 \pm 0.04\ \mu_B$ ($\chi_M T = 2.998-2.911\ cm^3\ K\ mol^{-1}$). Below 30 K the magnetic moment decreases reaching a value of $\mu_{eff} = 3.82\ \mu_B$ at 2 K. This is a clear indication that the antiferromagnetic exchange interaction between the Cr(III) and Ni(II) centers is negligibly small, if present at all. The solid line in Figure 4 represents the best fit with the following parameters: $J = 0$; $g_{Cr} = 1.98$; $g_{Ni} = 2.16$; $\Theta = -1.42$ K. Interestingly, most of the known Cr(III)−Ni(II) interactions in the literature are, in accord with the predictions made nearly 30 years ago, ferromagnetic in nature.[8,9]

The particular pairs of Cr(III)−Ni(II) complexes as well as the Cr(III)−Cu(II) species are classical examples for intramolecular ferromagnetic coupling which is predominantly due to the orthogonality of the magnetic orbitals. The *tris(pyridineal-doximato)-bridged Cr(III)−Ni(II) complexes,* **4** *and* **8**, *are rare examples of weak antiferromagnetic[10,11,28] or no coupling at all between the mentioned paramagnetic centers.*

At this stage it is tempting to search for a qualitative rationale for the trend and the nature of the exchange interactions between the spin carriers in the $Cr^{III}M^{II}$ pairs (M = Cr^{II} (**1**), Mn^{II} (**2**), Ni^{II} (**4** and **8**), Cu^{II} (**5**)) on the basis of the established Goodenough−Kanamori rules[37] for superexchange as presented concisely by Ginsberg[8b] and later by Kahn.[35] This will be performed by considering the symmetry of the molecule within the framework of localized spins. On the basis of the crystal structure analyses of **2**−**5**, **7**, and **8**, the molecular symmetry of the $Cr^{III}M$ pairs can be idealized to a C_3 point group.

Considering the O and N atoms of the bridging oxime groups as sp^2 hybridized in the network $Cr(O-N)_3M$, we will analyze the interactions evaluated from the magnetic data. Hence, we will consider the different possible interactions[38] of the sp^2 orbitals on either side of the bridging oximate ligands with the different metal orbitals in idealized C_3 symmetry. The five metal d orbitals with the 3-fold axis as the *z*-axis along the Cr···M vector transform in C_3 symmetry as a(d_{z^2}), 1e($d_{x^2-y^2}$, d_{xy}), and 2e(d_{yz}, d_{xz}), where orthogonality is prevailing only between a and 1e and a and 2e.

For complex **1**, $Cr^{III}Cr^{II}$, with the d^3d^4(hs) electronic configuration, it is evident from the exchange coupling constant *J* of $-7.9\ cm^{-1}$ that the dominant exchange pathways for **2** are the symmetry-allowed a||sp^2||a and 1e||sp^2||1e (using Ginsberg's symbols[8b]) σ-superexchange pathway.

Now, on going to the $Cr^{III}Mn^{II}$ species, **2**, in which the fifth electron of Mn^{II} occupies an empty 2e orbital, the overall interaction changes its nature from antiferromagnetic to weak ferromagnetic ($J = +1.5\ cm^{-1}$). Thus, the contribution of the path 2e||sp^2||2e to the overall interaction becomes very important, since the 2e orbitals centered on chromium and manganese are empty or half-filled, respectively, leading to ferromagnetic interactions.

Table 7. Simulated EPR Data for **3**, **6**, and **7**

	g_x^{eff}	g_y^{eff}	g_z^{eff}	W_x (G)	W_y (G)	W_z (G)
$Cr^{III}Fe^{II}$ (**3**)	3.88	3.86	1.97	310	300	350
$Cr^{III}Co^{III}$ (**7**)	3.90	3.88	1.97	150	250	100
$Cr^{III}Zn^{II}$ (**6**)	3.88	3.87	1.97	150	250	100

Next we turn to the d^3d^8 case in **4**, $Cr^{III}Ni^{II}$. The antiferromagnetic contribution provided by the 1e||sp^2||1e exchange path now exceeds those from all other ferromagnetic interactions, leading to an effective antiparallel spin coupling. Complex **4** is one of the very few examples[10,11,28] of antiferromagnetic interaction prevailing between six-coordinated Cr(III) and Ni(II). Interestingly, the second $Cr^{III}Ni^{II}$ species **8** exhibits no exchange interaction ($J = 0$). The crystallographic data of **8** indicate that both twist angle ϕ and dihedral angle θ, given in Table 5, for **8** are more twisted toward trigonal prismatic in comparison to those for **4**. Hence, the nature of the exchange interaction and its magnitude in the triply bridged $Cr^{III}Ni^{II}$ pair is expected to be a function of both ϕ and θ. It is to be mentioned that a triply oxime bridged $Cr^{III}Ni^{II}Cr^{III}$ species[28] with a twist angle of 24°, which is between those for **4** and **8**, exhibits a very weak antiparallel interaction ($J = -0.7\ cm^{-1}$).

Interestingly, occupancy of the 2e orbital of Cu(II) by one more single electron, thus reducing the number of unpaired electrons to one in the 2e orbital, results in weakening of the antiparallel path 1e||sp^2||1e (which is strong in case of $Cr^{III}Ni^{II}$), thus yielding an overall parallel spin coupling for **5**, $Cr^{III}Cu^{II}$.

We realize that the above description of the orbital pathways is based on a very simplified model. The network Cr−O−N−M is not linear, and it is oriented in different ways for structurally characterized pairs, thus leading to mixing-up of the metal d orbitals, which makes the picture more complex.

EPR Studies. X-band EPR spectra of **2**−**7** were recorded in CH_3CN solutions at low temperature (3−50 K) to establish the electronic ground state of the heterodinuclear complexes. Significant contributions from excited states were observed in the measured temperature range, due to weak exchange splitting of the spin states. This is consistent with the magnetic susceptibility measurements.

To determine the *g*-values for the $S = 3/2$ systems, EPR spectra of $Cr^{III}Fe^{II}$(ls) (**3**), $Cr^{III}Zn^{II}$ (**6**), and $Cr^{III}Co^{III}$(ls) (**7**) in CH_3CN solution were recorded at 4 K. The EPR spectra exhibit signals at $g_{||} = 1.97$ and $g_{\perp} = 3.88$ in full conformity with an $S = 3/2$ system with negligible rhombicity. The X-band EPR spectra of **3**, **6**, and **7** were simulated[39] by using the effective spin-Hamiltonian for an isolated $S = 3/2$ manifold. In Figure 5 this is demonstrated for **6**. The parameters obtained from the simulations are listed in Table 7. Thus $\langle g \rangle$ for Cr(III) in **3**, **6**, and **7** of 1.96 is in accord with the *g*-value obtained from the solid-state magnetic susceptibility measurements.

Interestingly, the integer spin system ($S_t = 4$) of **2**, $Cr^{III}Mn^{II}$, is EPR active, which reveals weak zero-field splitting within the spin multiplets. The EPR spectrum of **2** in CH_3CN at 10 K is depicted in Figure 6. The resonances of the solution spectra are broad and extend over a wide range from zero to more than 500 mT. The wide distribution of integer spin signals indicates that, under experimental conditions of X-band EPR, zero-field interaction and Zeeman interaction are comparable and correspond to the energy of X-band resonances ($h\nu = 0.3\ cm^{-1}$). Under these conditions magnetic substates are severely mixed and level splitting depends strongly on field strength and field

(36) (a) Journaux, Y.; Kahn, O.; Zarembowitch, J.; Galy, J.; Jaud, J. *J. Am. Chem. Soc.* **1983**, *105*, 7585. (b) Glerup, J.; Goodson, P. A.; Hodgson, D. J.; Lynn, M. H.; Michelsen, K. *Inorg. Chem.* **1992**, *31*, 4785. (c) Zhong, Z. J.; Matsumoto, N.; Okawa, H.; Kida, S. *Inorg. Chem.* **1991**, *30*, 436. (d) Andruh, M.; Melanson, R.; Stager, C. V.; Rochon, F. D. *Inorg. Chim. Acta* **1996**, *251*, 309. (e) Costes, J.-P.; Dahan, F.; Dupuis, A.; Laurent, J.-P. *J. Chem. Soc., Dalton Trans.* **1998**, 1307 and references therein.

(37) (a) Goodenough, J. B. *Magnetism and the Chemical Bond*; Wiley: New York, 1963. (b) Goodenough, J. B. *J. Phys. Chem. Solids* **1958**, *6*, 287. (c) Kanamori, J. *J. Phys. Chem. Solids* **1959**, *10*, 87.

(38) (a) Kettle, S. F. A. *Symmetry and Structure*; Chichester, U.K., 1985. (b) Krishnamurthy, R.; Schaap, W. B. *J. Chem. Educ.* **1969**, *46*, 799. (c) Albright, T. A.; Burdett, J. K.; Whangbo, M.-H. *Orbital Interactions in Chemistry*; John Wiley & Sons: New York, 1985.

(39) Krebs, C. EPR-simulation program GEFIT. Dissertation, Ruhr-Universität Bochum, Bochum, Germany, 1997.

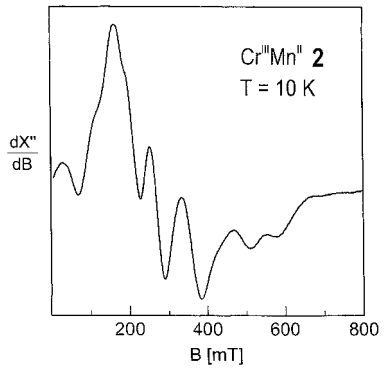

Figure 6. EPR spectrum of **2**, $Cr^{III}Mn^{II}$, in CH_3CN at 10 K (microwave frequency 9.45 GHz; power 100.6 μW; modulation amplitude 12.5 G).

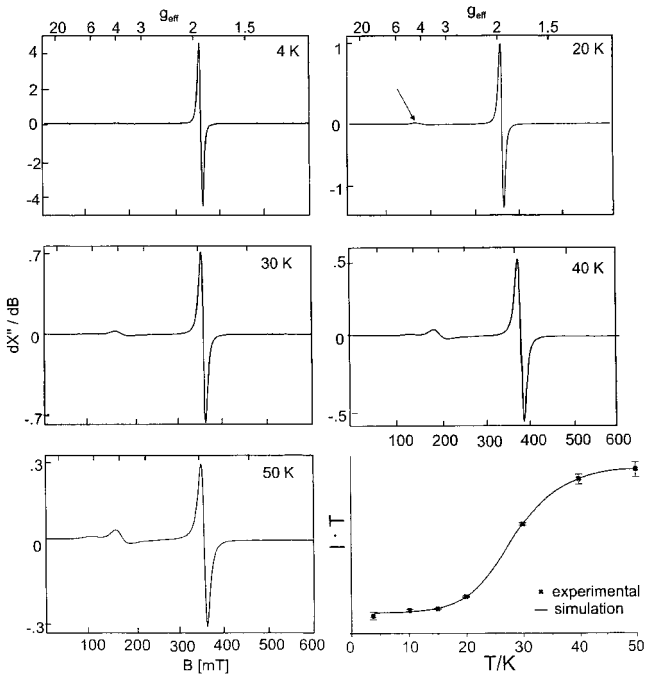

Figure 7. EPR spectra of **4**, $Cr^{III}Ni^{II}$, in CH_3CN recorded as a function of temperature in the range 4−50 K (microwave frequency 9.45 GHz; microwave power 100.6 μW; modulation amplitude 12.5 G). Bottom: Temperature dependence of the temperature-weighted intensity of the signal at $g \sim 2$. The solid line is the calculated Boltzmann function with $J = -9$ cm^{-1}.

direction within the molecular frame. The EPR resonances, therefore, depend on the orientation of molecules in frozen solution and, hence, are spread over a wide range of applied fields. From such complex integer spin EPR spectra, **g** tensors of the spin manifolds cannot be derived without explicit simulations.

Complex **5**, $Cr^{III}Cu^{II}$, with an apparently integer spin ground state ($S_t = 2$) is EPR silent under our experimental conditions, indicating clearly strong zero-field interaction ($D \gg h\nu$).

The X-band EPR spectrum of **4**, $Cr^{III}Ni^{II}$, in CH_3CN in the temperature range 4−15 K exhibits a signal for $S_t = 1/2$ with $g = 1.88$. The intensity of the signal decreases, and an additional signal at "$g \approx 4$" grows in with increasing temperature (Figure 7). The variation of the temperature-weighted data (intensity × temperature vs temperature) is typical of excited-state resonances coming from a manifold well above the ground state $S_t = 1/2$. Figure 7 shows the values that are obtained in the range 4−50 K by double integration of the experimental derivative signals at "$g \approx 2$" measured under nonsaturating conditions. The solid line in the plot of I·T vs T of Figure 7 is a fit with the Boltzmann function

$$IT\alpha \frac{\exp\{-3|J|/kT\}}{Z}$$

for the $S_t = 3/2$ manifold with $Z = [1 + 2\exp\{-3|J|/kT\} + 3\exp\{-8|J|/kT\}]$ being the corresponding partition function and $J = -9 \pm 3$ cm^{-1}. Hence, this J value based on the EPR intensity data obtained from frozen solutions and the magnetic susceptibility result for solid material ($J = -9.2$ cm^{-1}) are consistent with each other and prove the *intramolecular* nature of the exchange interaction. Additionally, using $g_{Cr} = 2.0$ and $g_{Ni} = 2.193$ obtained from the static magnetization measurement on solid material, $g_{|1/2>}$ can be easily calculated to be 1.87, which is in complete agreement with the ground-state g-value obtained for 4 at 4 K by EPR.

Concluding Remarks

To conclude, the following points of this study deserve particular attention:

(i) Tris(pyridine-2-aldoximato)metalates are capable of acting as ligands to give rise to various dinuclear complexes containing oximato groups (═N−O) as bridging ligands, which can mediate exchange interactions of varying range.

(ii) Spin coupling between the ions Cr^{III} and Ni^{II} (d^3d^8 system) can be antiferromagnetic in nature, in contrast to the generally expected ferromagnetic coupling between the said spin carriers in a 6-coordinated environment. Antiferromagnetic spin coupling has been demonstrated both by susceptibility and EPR measurements.

The common strategy of obtaining ferromagnetically coupled bimetallic systems through involvement of symmetry-related strict orthogonality of the magnetic orbitals of the interacting metal centers, viz. the $t_{2g}^3(Cr) \perp e_g^2(Ni)$ interactions for **4** and **8**, does not lead to the expected results for the triply bridged $Cr^{III}Ni^{II}$ systems, presumably due to the mixing of five metal d orbitals in trigonal symmetry, which provides several exchange components opposite in nature; thus, a bulk weak to negligible spin exchange interactions result. Hence, the idea of using triply bridged $Cr^{III}Ni^{II}$-pairs to produce ferromagnetic building blocks for obtaining high-spin molecules does not seem to be very promising.

Considering the triply oxime-bridged $Cr^{III}Ni^{II}$ compounds, **4** and **8**, and the $Cr^{III}Ni^{II}Cr^{III}$ compound described earlier,[28] no simple relationship between the trigonal twist angle θ, the Cr···Ni distances, and the exchange coupling constant J is observed.

(iii) The investigation emphasizes the observation of a well-resolved $S_t = 4$ EPR spectrum, arising from the parallel spin coupling in **2**, $Cr^{III}Mn^{II}$.

(iv) Electrochemical measurements indicate redox processes centered on the ligand pyridine-2-aldoxime (PyA). Thus the oxime ligand can give rise to PyA-based both cation and anion radicals.

No stabilization of the Ni(IV) state in **4** and **8** by the oxime ligands has been observed.

Acknowledgment. The work was partly supported by the Fonds der Chemischen Industrie.

Supporting Information Available: Figures S1−S3 and X-ray crystallographic files in CIF format. This material is available free of charge via the Internet at http://pubs.acs.org.

IC010552Y